

ULTRA-COMPACT DWARFS IN THE CORE OF THE COMA CLUSTER ¹

JUAN P. MADRID², ALISTER W. GRAHAM², WILLIAM E. HARRIS³,
PAUL GOUDFROOIJ⁴, DUNCAN A. FORBES², DAVID CARTER⁵, JOHN P. BLAKESLEE⁶,
LEE R. SPITLER², HENRY C. FERGUSON⁴

ApJ accepted

ABSTRACT

We have discovered both a red and a blue subpopulation of Ultra-Compact Dwarf (UCD) galaxy candidates in the Coma galaxy cluster. We analyzed deep F475W (Sloan *g*) and F814W (I) Hubble Space Telescope images obtained with the Advanced Camera for Surveys Wide Field Channel as part of the Coma Cluster Treasury Survey and have fitted the light profiles of ~ 5000 point-like sources in the vicinity of NGC 4874 — one of the two central dominant galaxies of the Coma cluster. Although almost all of these sources are globular clusters that remain unresolved, we found that 52 objects have effective radii between ~ 10 and 66 pc, in the range spanned by Dwarf Globular Transition Objects (DGTO) and UCDs. Of these 52 compact objects, 25 are brighter than $M_V \sim -11$ mag, a magnitude conventionally thought to separate UCDs and globular clusters. The UCD/DGTO candidates have the same color and luminosity distribution as the most luminous globular clusters within the red and blue subpopulations of the immensely rich NGC 4874 globular cluster system. Unlike standard globular clusters, blue and red UCD/DGTO subpopulations have the same median effective radius. The spatial distribution of UCD/DGTO candidates reveal that they congregate towards NGC 4874, and are not uniformly distributed. We find a relative deficit of UCD/DGTOs compared with globular clusters in the inner 15 kpc around NGC 4874, however at larger radii UCD/DGTO and globular clusters follow the same spatial distribution.

Subject headings: star clusters - galaxies: elliptical and lenticular, cD - globular clusters: general

1. INTRODUCTION

Within galaxy clusters, cD galaxies are swarming with tens of thousands of globular clusters. Like most galaxies with rich Globular Cluster Systems (GCS), the cD galaxies of Virgo (M87: Peng et al. 2009; Harris 2009b) and Fornax (NGC 1399: Dirsch et al. 2003) display evident bimodality in their color distribution. Bimodal fits to the GCS around NGC 3311, the central cD galaxy of the Hydra galaxy cluster, also reveal the presence of a red (metal-rich) and a blue (metal-poor) subpopulation (Wehner et al. 2008). Six additional giant elliptical galaxies studied by Harris (2009a) also show clear bimodality.

In the analysis of the color-magnitude diagram (CMD) of the NGC 3311 GCS, Wehner & Harris (2007; their Figure 1) find an "upward" extension towards brighter magnitudes of the red subpopulation. This continuation to brighter magnitudes (and higher masses) is absent among the blue subpopulation. Wehner & Harris (2007) postulate that given their magnitudes ($i' \leq 22.5$

mag) and inferred masses ($> 6 \times 10^6 M_\odot$), the extension of the CMD corresponds to Ultra-Compact Dwarfs (UCDs, Phillipps et al. 2001). While Wehner & Harris (2007) suggest that UCDs are the bright extension of the GCS, the ground-based data used for their work do not allow them to derive characteristic radii for their UCD candidates. Peng et al. (2009) over-plotted 18 objects with extended effective radii ($r_h > 10$ pc) on their CMD of the M87 GCS. Some of these objects are confirmed UCDs or Dwarf/Globular Transition Objects (Hasegan et al. 2005) and most of them lie exactly at the bright end of the blue subpopulation of globular clusters.

Ultra-compact dwarfs are a relatively newly discovered class of stellar system (Hilker et al. 1999; Drinkwater et al. 2000) and their origin is not yet clearly established. In color, and structural parameters, UCDs lie between supermassive globular clusters and compact dwarf elliptical galaxies. Not surprisingly, the origin of UCDs has been linked to both globular clusters and dwarf elliptical galaxies (Hilker 2006, and references therein). UCDs are typically associated with galaxy clusters and were originally identified in the Fornax cluster (Hilker et al. 1999; Drinkwater et al. 2000, 2003). Subsequently, the presence of UCDs was reported in several additional galaxy clusters: Virgo, Centaurus, Hydra, Abell S040 and Abell 1689 (Evstigneeva et al. 2008; Chilingarian & Mamon 2008; Mieske et al. 2004, 2007; Wehner & Harris 2007; Blakeslee & Barber DeGraaff 2008). However, Romanowsky et al. (2009) report the presence of UCDs in the galaxy group hosting NGC 1407. Most recently, a spectroscopically confirmed UCD in the low density environment surrounding the Sombrero Galaxy was discovered by Hau et al. (2009). UCDs are difficult to find since

¹ Based on observations made with the NASA/ESA Hubble Space Telescope, obtained at the Space Telescope Science Institute, which is operated by the Association of Universities for Research in Astronomy, Inc., under NASA contract NAS5-26555. These observations are associated with program 10861.

² Centre for Astrophysics and Supercomputing, Swinburne University of Technology, Hawthorn, VIC 3122, Australia

³ Department of Physics and Astronomy, McMaster University, Hamilton, ON L8S 4M1, Canada

⁴ Space Telescope Science Institute, 3700 San Martin drive, Baltimore, MD 21218, USA

⁵ Astrophysics Research Institute, Liverpool John Moores University, Egerton Wharf, Birkenhead, UK

⁶ Herzberg Institute of Astrophysics, Victoria, BC V9E 2E7, Canada

they are often mistaken for stars, or simply bright globular clusters, and their structural parameters can only be derived using the Hubble Space Telescope. The formation of UCDs and possible links between UCDs and globular clusters (either red or blue) remains a subject of debate.

We analyze high resolution Advanced Camera for Surveys (ACS) data of the core of the Coma cluster, the richest galaxy cluster in the nearby Universe (Colless 2001). The Coma cluster provides the unique opportunity to study a very large number of distinct galaxies within a small area of the sky, as shown in Figure 1. Coma contains a diverse sample of stellar systems ranging from globular clusters to giant elliptical galaxies. The core of this cluster contains two giant elliptical galaxies (NGC 4874 and NGC 4889) with globular cluster systems that, when combined, have more than 30000 members (Blakeslee & Tonry 1995; Harris et al. 2009). We specifically study an ACS pointing containing NGC 4874, one of the two central galaxies of Coma, and the only central galaxy with ACS imaging. The globular cluster system of NGC 4874 alone has an estimated *minimum* of 18700 members (Harris et al. 2009), the largest published globular cluster system.

We derive a color-magnitude diagram for this immense GCS allowing us to clearly define its color distribution. We also estimate the structural parameters of sources that show extended structure using ISHAPE (Larsen 1999), a specially designed software to derive the structural parameters of slightly resolved astronomical objects. We find that 52 objects have effective radii $\gtrsim 10$ pc. These objects have colors, and magnitudes similar to the brightest globular clusters. We postulate that these objects constitute the UCD and DGTO population of the core of the Coma Cluster.

There is a vast terminology to define objects larger than GCs and smaller than dwarf elliptical galaxies: Intermediate Mass Object, Dwarf Galaxy Transition Object, super-massive star cluster, etc. (see Hilker 2006 for a review). UCDs, in particular, are conventionally defined as objects with radii of ~ 10 -100 pc, although departures from this size range have been reported (e.g. Evstigneeva et al. 2008). A commonly quoted lower limit for the mass of UCDs is $2 \times 10^6 M_{\odot}$ (Mieske et al. 2008) and their magnitude limit is typically $M_V \lesssim -11$ mag (Mieske et al. 2006). UCDs also have higher mass-to-light ratios than globular clusters and the presence of dark matter in these stellar systems is still under debate (Hasegan et al. 2005; Dabringhausen et al. 2008). In this paper we will refer to the ensemble of 52 objects with an effective radius $\gtrsim 10$ pc as UCD/DGTOs. The term UCDs will be reserved for the subset of 25 objects which are additionally brighter than the luminosity requirement for the UCD label.

Independent methods give estimates of the distance to the Coma cluster between 84 and 108 Mpc, see Table 1 of Carter et al. (2008). We adopt a fiducial distance of 100 Mpc and thus a scale of 23 pc per $0.05''$ (one ACS pixel).

2. DATA

We use data taken during the Coma Cluster Survey (Carter et al. 2008). This HST Treasury program was able to obtain eighteen pointings of the core of the Coma Cluster with the ACS Wide Field Channel detector be-

fore the electronics failure of the instrument. Each field comprises imaging in two different filters: F475W (similar to Sloan *g*) and F814W (Cousins I) (Mack et al. 2003).

The science data from this observing program were prepared through a dedicated pipeline that is described in detail by Carter et al. (2008). The final images were created using the PYRAF task MULTIDRIZZLE (Koekemoer et al. 2002). We use the public data products from the second release of the Coma Cluster Treasury program which provide the best relative alignment between the two filters. In the nomenclature of the second data release, we use field number 19 with target name Coma 3-5. The exposure times for this field are 2677 s and 1400 s for the F475W and F814W filters, respectively.

3. PSF

We build the PSF using the DAOPHOT package within PYRAF. We perform photometry of candidate stars using the task PHOT, the selection of optimal stars is carried out using PSTSELECT which selects 12 bright, uncrowded, and unsaturated stars across the field. The computation of a luminosity weighted PSF is done with the task PSF. ISHAPE requires the PSF to be oversampled by a factor of ten, that is the pixel size should be a tenth of the native pixel size of the science image. We create an oversampled PSF with the task SEEPSF, and we provide the resulting PSF as input to ISHAPE. While several options to calculate the PSF for the HST exist, it has been shown that with the sequence of DAOPHOT tasks described above a reliable and accurate model of the PSF core can be constructed (Spitler et al. 2006; Price et al. 2009).

4. DETECTION

We median filter the images in both bands with a box size of 41×41 pixels and then subtract the result from the original images to obtain a residual free of galaxy light. We thus facilitate the detection of the position of point-like sources. A first catalogue of sources is generated running SExtractor (Bertin & Arnouts 1996) on the image created by adding the median-subtracted images of the two filters. Within SExtractor we use a detection threshold of 3σ with a minimum of five pixels above the threshold to trigger an extraction. A lower detection limit would generate a large number of spurious detections while more conservative parameters would leave globular clusters undetected.

We perform a first round of careful visual inspection of all detections and eliminate spurious sources such as background galaxies and objects along the edge of the chip. We use a novel method to carry out a secondary visual inspection of our 4976 remaining detections. We take advantage of the short computation time needed to derive an initial set of structural parameters with ISHAPE. In order to discard spurious sources from our analysis we follow the steps described below. With the initial set of structural parameters obtained with ISHAPE we create a list of objects with dubious values such as very large ellipticity or conspicuously large effective radii ($r_h \gtrsim 100$ pc) for visual inspection. By virtue of the high-resolution imaging of the ACS we can determine that most of these objects are background galaxies, irregular structures, or gradients of surface brightness without link to any real source. Examples of objects flagged and eliminated due

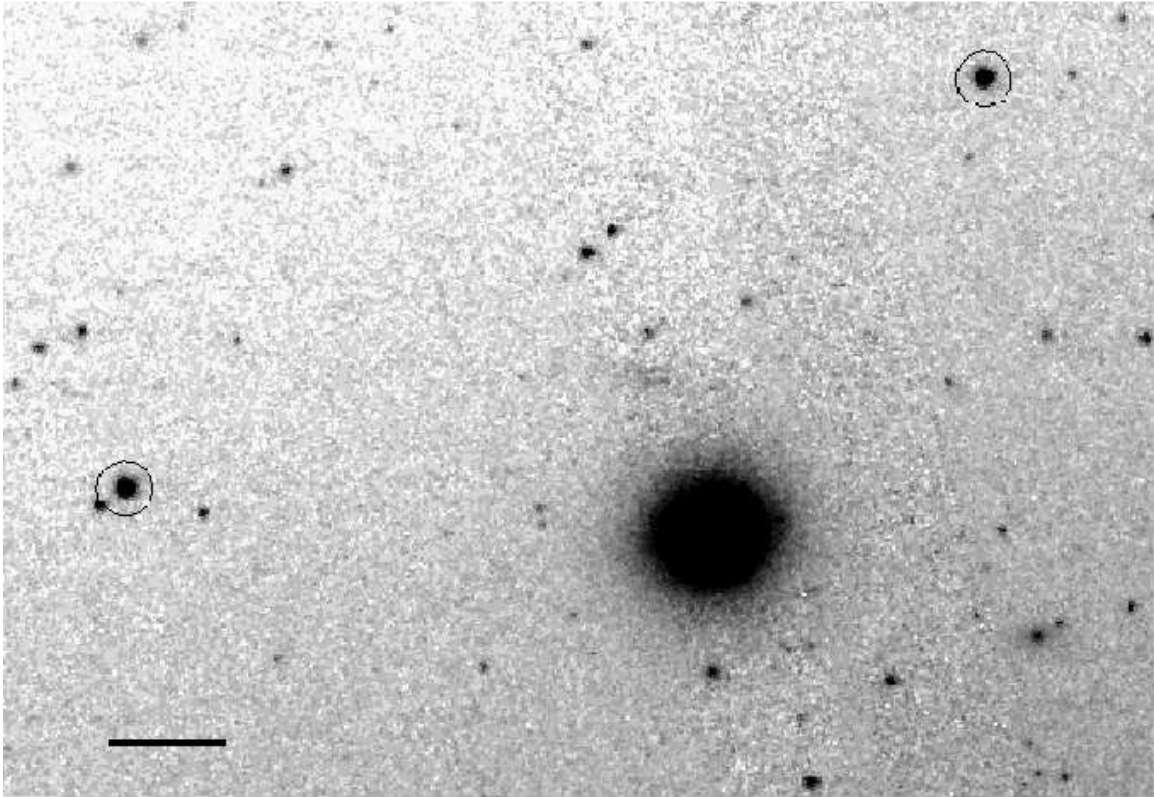


FIG. 1.— Section of the HST/ACS image illustrating the rich diversity of stellar systems in the core of the Coma cluster. The brightest galaxy is CcGV19a, classified as a compact elliptical by Price et al. (2009). Two UCD candidates are indicated with circles. Several members of the rich globular cluster system of NGC 4874 are also clearly visible. The center of this image is located at ~ 24 kpc NE from NGC 4874. The diffuse halo of this central dominant galaxy is apparent as a diagonal light gradient across the field of view from bottom right to top left. The bar on the lower left is 1 kpc in length. North is up and east is left.

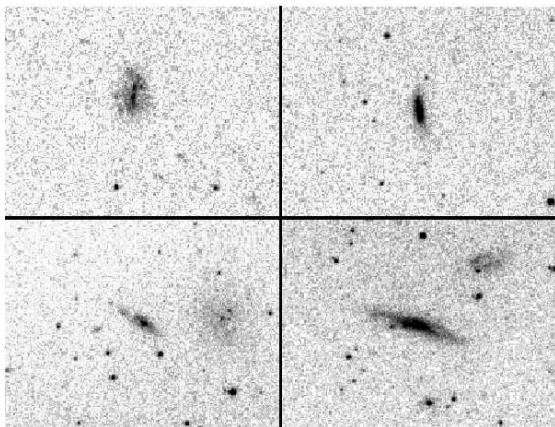


FIG. 2.— Four examples of spurious detections eliminated based on their suspicious structural parameters. These sources are background galaxies in all likelihood and have effective radii that would correspond to hundreds of parsecs if they were at the distance of Coma.

to their suspicious structural parameters (i.e. large ellipticity or large effective radius) are presented in Figure 2. Using this method we are able to eliminate 170 false detections in a short time. We are left with 4806 sources, most of them globular clusters belonging to the NGC 4874 GCS.

5. STRUCTURAL PARAMETERS

5.1. *Effective radius*

The high resolution of the Hubble Space Telescope has enabled the measurement of structural parameters

of vast numbers of extragalactic globular clusters. Using WFPC2 data, Larsen et al. (2001) derived size estimates from globular clusters of seventeen nearby, early-type galaxies and found that the majority of clusters have effective radii of two to three parsecs. Based on ACS data, and an independent technique, Jordán et al. (2005) derived the effective radii of thousands of globular clusters from 100 early-type galaxies in the Virgo cluster and report a median GC effective radius of 2.7 pc. Masters et al. (2010), studying the globular clusters around 43 early-type galaxies in the Fornax cluster found that the median r_h of a GC is 2.9 pc. These results are in remarkable agreement with size measurements of GCs in spirals (Spitler et al. 2006; Harris et al. 2010) and with the known median effective radii of Galactic globular clusters, i. e. $\langle r_h \rangle = 3.2$ pc (Harris et al. 1996). At present, no correlation has been found between the luminosity (or mass) of globular clusters and their effective radius, however their median r_h is ~ 3 pc.

We fit the light profiles of 4806 sources using ISHAPE (Larsen 1999), a software commonly used to derive the structural parameters of barely resolved astronomical objects, such as, extragalactic globular clusters. ISHAPE convolves the point-spread function (PSF) with an analytical model of the surface brightness profile and searches for the best fit to the data by varying the full width half maximum (FWHM) of the synthetic profile. The output given by ISHAPE for each source comprises the effective radius (or equivalently half-light radius), the ratio of the minor over major axis, the position angle, the

signal-to-noise level, and the reduced χ^2 (or goodness of fit).

Within ISHAPE the user can choose among several analytical models for the light profile that will be used during the fitting process, e.g. King, Sérsic, Gaussian. We adopt a King profile with a concentration parameter of $c = 30$; the concentration parameter c is defined as the ratio of the tidal radius over the core radius $c = r_t/r_c$ (King 1962, 1966).

The value of $c = 30$ accurately represents the average concentration parameter for Milky Way, M31, and NGC 5128 globular clusters (Harris et al. 1996; Harris 2009a and references therein). Moreover, the concentration parameters for UCDs in Fornax and Virgo derived by Evstigneeva et al. (2008) are consistent with a choice of $c = 30$. In addition, by using $c=30$ we facilitate comparison with similar studies e.g. Blakeslee & Barber DeGraaff (2008). Also, quantitative tests show that for partially resolved objects the solution for r_h is very insensitive to the particular choice of c (Harris et al. 2010).

A signal-to-noise ratio of $S/N > 50$ is necessary to obtain reliable measurements of the structural parameters with ISHAPE. This requirement for the S/N was demonstrated through extensive testing of ISHAPE by Harris (2009a). Of our initial 4806 sources for which we derived structural parameters, 631 sources conform to this S/N requirement simultaneously in both bands. Hereafter, when considering structural parameters we will refer only to those 631 objects with $S/N > 50$ in both bands.

At the distance of the Coma cluster, namely 100 Mpc, the effective radius of a globular cluster (~ 3 pc) is equivalent to six milliarcseconds, a radius practically irrecoverable in ACS/WFC data with a pixel size of $0.05''$. Using WFPC2 data, Harris et al. (2009a) demonstrated that at the distance of Coma objects with $r_h < 6$ pc have light profiles indistinguishable from those of stars. As expected, the vast majority of clusters for which we attempted to obtain reliable structural parameters remain unresolved and thus an estimate of their effective radius cannot be made, see Figure 3. However, with ISHAPE we find 52 sources that are positively resolved.

We derive the structural parameters of all sources independently in both bands. We minimize systematics between the two measurements by strictly following the same set of steps. We also use the same set of stars to create both PSFs. In Figure 3 we present the ratio $\frac{r_{h,F475W}}{r_{h,F814W}}$ plotted against $r_{h,F814W}$. This figure shows how the ratio converges to ~ 1 at $r_{h,F814W} > 9$ pc. At larger radii (> 10 pc) the agreement between the two measurements is excellent and reveals a small but real offset. This small but significant difference (12%) in the value of r_h in these two bands can be expected due to physical reasons, notably color gradients within globular clusters (Larsen et al. 2008). These authors find that r_h can vary by up to 60% between the measurements in blue (F333W) and red (F814W) bands. For our measurements of UCD/DGTOs the median of the ratio $\frac{r_{h,F475W}}{r_{h,F814W}}$ is $\mu = 0.88^{+0.03}_{-0.02}$.

We select as UCD/DGTO candidates only those objects that are resolved in *both* bands. The vertical line in Figure 3 shows that all objects with $r_{h,F814W} \geq 9.2$ pc are consistently resolved in both bands. Most of the UCD/DGTO candidates (45 of them) have an effective radius larger than 10 pc in at least one band, the min-

imum size commonly quoted for UCDs (Mieske et al. 2004). We include in our list of candidates seven objects slightly below this, somehow arbitrary, cut: these seven objects have an $r_h \geq 9.5$ in one band and are within the errors ($\pm 0.006''$ or ± 2.8 pc, Harris 2009a) in agreement with the standard size definition of UCDs. Objects resolved in one band but having zero size in the other are rejected as UCD/DGTO candidates, see Figure 3.

We also explore the impact of the fitting radius in pixels (FITRAD) that we use as an input of ISHAPE. The UCD candidates are barely resolved in the ACS images, that is, they have a FWHM of ~ 3 pixels. ISHAPE is limited to a fit radius of a few pixels (Blakeslee & Barber DeGraaff 2008) and the optimal fitting radius is the result of a balance between signal and noise, similar to the evolution of the S/N ratio as a function of aperture radius in photometric measurements. The selection of candidates is carried out using a FITRAD=6 pixels. The consistency of the measurements with FITRAD=6 pixels is shown in Figure 3 where we compare the values of r_h in both bands.

ISHAPE yields robust values of effective radius independent of the model selected by the user i.e. the value of r_h measured with a King profile is expected to be similar to r_h obtained using a Sérsic profile. We exploit this property of ISHAPE in Figure 4. The aim of Figure 4 is twofold: we show the impact on the value of r_h measured by ISHAPE of i) two different analytical models, ii) two different fitting radii. The values of r_h returned by ISHAPE should be equivalent for different (but reasonable) analytical models of the surface brightness profile. In fact, a King profile (King 1962, 1966) with a concentration parameter of $c=30$, and a Sérsic model (Sérsic 1968) with a Sérsic index of $n = 2$ are equivalent for our measurements. This is particularly true for the smaller UCD candidates as noted by Evstigneeva et al. (2008). A larger fitting radius, FITRAD=15 pixels instead of FITRAD=6 pixels, gives generally a larger r_h . Given that a larger fitting radius is more appropriate for bigger sources, we report in Table 1 the values obtained using FITRAD=15 pixels for those sources with $r_h > 25$ pc in the initial run with FITRAD=6 pixels.

Globular clusters have a median r_h of ~ 3 pc but their size distribution extends up to eight parsecs (Harris 2009a, Masters et al. 2010). UCDs studied by Evstigneeva et al. (2008) range in r_h between 4.0 and 93.2 pc while Blakeslee & Barber DeGraaff (2008) report UCDs with r_h ranging from 11.2 to 90.3 pc with a tentative gap between large globular clusters (or the most compact UCDs) with $r_h < 20$ pc and large UCDs with $r_h > 40$ pc. We find objects with r_h almost continuously spanning the range from 10 to 40 pc, we find no indication for a break in the size distribution of these compact stellar systems.

Metal-poor globular clusters are on average $\sim 25\%$ larger than metal-rich ones. This size difference has been well documented by several studies (Jordán et al. 2005; Spitler et al. 2006, Harris 2009a; Masters et al. 2010). This size difference has been explained as the result of mass segregation combined with the metallicity dependence of main sequence stars (Jordán 2004). Harris (2009a) postulates that the conditions of formation can also be responsible for this size difference while Larsen & Brodie (2003) argue that a size-galactocentric distance

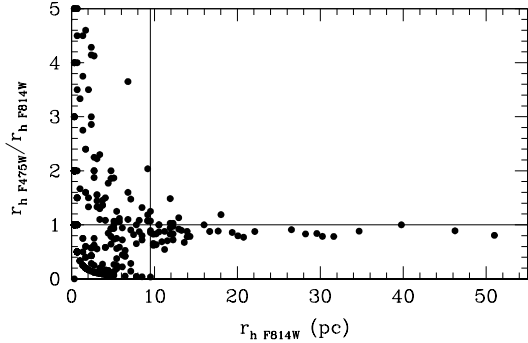


FIG. 3.— Ratio of r_h in the two bands vs. r_h in the F814W filter for all systems with $S/N > 50$ (FITRAD=6 PIXELS). This plot reveals how standard globular clusters cannot be resolved at the Coma distance. On the other hand, all objects with $r_{h,F814W} \geq 9.2$ pc are consistently resolved in both bands as marked by the vertical line. Objects larger than 10 pc show an excellent agreement.

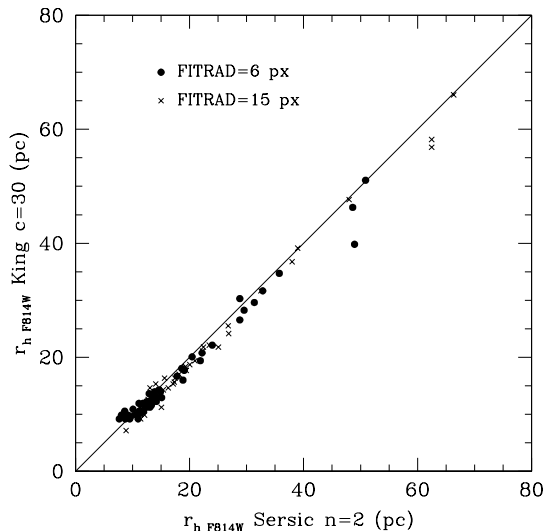


FIG. 4.— Effective radii measured by ISHAPE using different analytical models and different fitting radii (FITRAD, in pixels). The effective radius derived by ISHAPE using different analytical models shows excellent agreement. For the largest UCD candidates a larger fitting radius yields a larger effective radius.

trend and projection effects are the decisive factors. The correlation between size and color (or metallicity) observed for globular clusters is blurred at higher masses. In our sample blue UCD/DGTO candidates have a median effective radius of $12.2_{-0.5}^{+1.7}$ pc while the median r_h for red UCD/DGTO candidates is $11.9_{-0.6}^{+4.2}$ pc.

5.2. Ellipticity

ISHAPE computes the minor/major (b/a) axis ratio for each object. We use this ratio to derive the ellipticity ($\epsilon = 1 - b/a$) and to set a selection limit of $0 \leq \epsilon < 0.5$ for our UCD/DGTO candidates. Figure 5 shows the ellipticity values of our UCD/DGTO candidates which span the whole range set by our selection criterion. The smallest ellipticity of this sample is 0.03, only two candidates have an ellipticity of less than 0.1. Blakeslee & Barber DeGraaff (2008) found that all their UCD candidates have an ellipticity between 0.16 and 0.46. The largest ellipticity in our sample of UCD candidates is 0.49

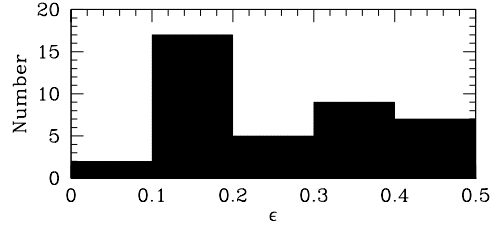


FIG. 5.— Ellipticity distribution for UCD/DGTO candidates. A peak in the distribution is evident at ~ 0.15 , and we find only two nearly spherical objects with $\epsilon < 0.1$, and the median of the distribution is 0.24.

The complete list of UCD/DGTO candidates with their effective radius and ellipticity is presented in Table 1. Given that ISHAPE measures the effective radius along the major axis, we apply a correction to obtain the circularized effective radius that we present in Table 1:

$$r_{h,circularized} = r_{h,ishape} \sqrt{(1 - \epsilon)}$$

6. PHOTOMETRY

We perform photometric measurements with the task PHOT of the PYRAF/DAOPHOT package. We execute aperture photometry with a four pixel radius and apply aperture correction following the formulas of Sirianni et al. (2005). We use the ACS/WFC Vega zero points for each filter that we obtain from the updated tables maintained by the STScI, i.e. $m_{F475W} = 26.163$ mag, and $m_{F814W} = 25.520$ mag (Sirianni et al. 2006). Note that the main catalogue of sources for the Coma Treasury Survey uses AB magnitudes (Hammer et al. 2010). Foreground Galactic extinction is calculated using $E(B-V) = 0.009$ mag (from NED) and the extinction ratios of Sirianni et al. (2005), from which we obtain $A_{F475W} = 0.032$ mag and $A_{F814W} = 0.016$ mag.

We obtain photometric measurements of 4806 sources in F475W and F814W. Most of these sources are globular clusters likely belonging to the NGC 4874 GCS. As shown in Figure 1, crowding is not an issue in our data.

6.1. Color-Magnitude Diagram

In the color-magnitude diagram of Figure 6 we also plot the size information derived with ISHAPE. Unresolved globular clusters belonging to the NGC 4874 GCS are plotted as black dots. Some of these globular clusters might also be intracluster globular clusters of Coma similar to those found in the Virgo cluster (Williams et al. 2007; Lee et al. 2010). UCD/DGTO candidates are plotted as filled red circles. Our UCD/DGTO candidates coincide in color with the brightest members of the metal-poor and metal-rich subpopulations of globular clusters.

The color distribution of the brightest GCs is clearly defined in the CMD. Background galaxies removed while cleaning spurious detections have different colors than globular clusters. This was demonstrated by Dirsch et al. (2003; their Figure 3) studying a field containing the NGC 1399 GCS and a background field; see also Harris (2009b) for his study of contamination in the M87 field. Moreover, evolutionary synthesis models predict that elliptical galaxies of any age, which are the background objects most likely to appear as UCDs, have colors $(B - I) > 1.9$ (Buzzoni 2005).

Mieske et al. (2004) set a magnitude limit of $M_V < -11.5$ mag for their UCD selection criteria while Hasegan

et al. (2005) adopt $M_V < -10.8$ mag. Mieske et al. (2006) identified a metallicity break and thus set the onset of the size-luminosity relation at $M_V < -11$ mag. Assuming $V - I = 1.1$ mag and a distance modulus to the Coma Cluster of $(m - M) = 35.0$ mag we find that UCDs should have $m_I < 22.9$ mag if we set a selection limit of $M_V < -11$ mag. We have assumed $I \approx F814W$ (Sirianni et al. 2005).

There are 110 objects in total with $m_{F814W} < 22.9$ mag in the color-magnitude diagram of Figure 6, i.e. above the horizontal bar, 25 of these objects also have effective radii characteristic of UCDs. These 110 objects are of similar or higher mass than ω Centauri ($2.5 \times 10^6 M_\odot$, van de Ven et al. 2006). Higher resolution data should reveal that the remaining 85 objects have an extended structure given that $\sim 2 \times 10^6 M_\odot$ marks the onset of a size-luminosity relation for stellar structures (Hasegan et al. 2005; Forbes et al. 2008; Murray 2009). We also present the color histogram in the bottom panel of Figure 6, which is consistent with the histogram presented by Harris et al. (2009).

6.2. Size-magnitude

We attempt to show the onset of the size luminosity relation in Figure 7. This figure is divided in four quadrants that are limited by the luminosity limit of UCDs and the ability of our data to obtain reliable size estimates i.e. a size of ~ 9.2 pc. Among the large scatter of the data points characteristic of such a plot (Masters et al. 2010; Forbes et al. 2008) we find that the fraction of unresolved stellar structures brighter than the minimum luminosity limit is particularly low around $m_{F814W} \sim 22$ mag, a *hint* of the onset of a size-luminosity dependence. More data points are needed to confirm this trend.

6.3. Color Bimodality

We use the software R for our statistical calculations presented in this work. R is a freely available, open source environment for statistical computing. The code RMIX, run within R, is specially designed to evaluate the mixture of multiple distributions within a histogram. RMIX is particularly well suited for the analysis of the underlying distributions present in the color-magnitude diagram. The code and its application to the analysis of a CMD has been presented, for example, by Wehner et al. (2008) and Harris (2009a).

The CMD of globular cluster systems is expected to be bimodal and, as noted earlier, for central dominant galaxies this bimodality should be evident. The bimodal UCD color distribution sits atop a bimodal globular cluster distribution well identified for GCs brighter than $F814W < 24$ mag, see both panels of Figure 8.

We use the best bimodal fit to the color distribution of the 52 UCD/DGTO candidates to estimate the color boundary between blue and red UCD candidates (Figure 8). We define this point as the intersection of the two Gaussians fitting each subpopulation (Peng et al. 2006). We thus set the boundary between blue and red UCD/DGTO candidates at $F475W - F814W = 1.61$. According to this fit, 63% of our UCD/DGTOs belong to the blue subpopulation, while 37% are red. For UCDs only (i.e. $M_V < -11$ mag), 44% of them are blue and 56% are red.

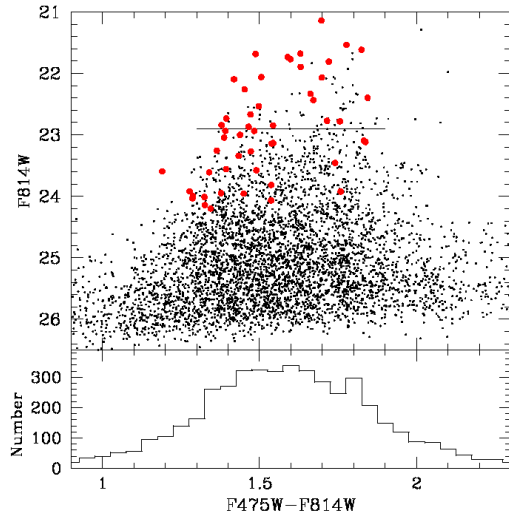


FIG. 6.— Top panel: Color-Magnitude Diagram of the globular cluster system and UCD candidates around NGC 4874. Unresolved globular clusters are plotted as black dots while resolved UCDs are shown as red circles. The horizontal bar marks $M_V = -11$ mag. Bottom panel: Color histogram for all globular clusters. The standard bimodality is blurred due to photometric uncertainties at faint magnitudes.

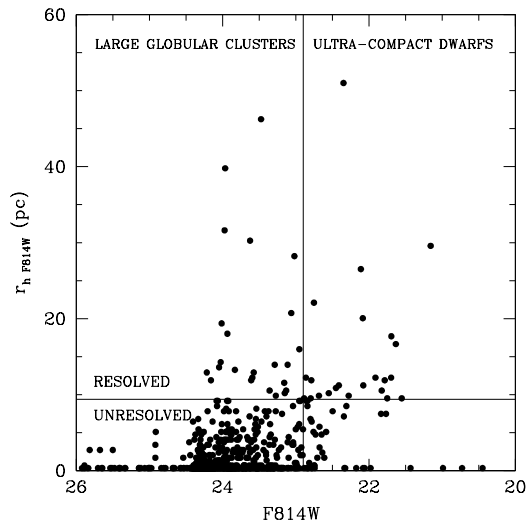


FIG. 7.— Magnitude versus effective radius for all objects with $S/N > 50$. This diagram is divided in four quadrants delimited by the minimum luminosity for UCDs and the ability of our data to resolve the compact stellar objects we study.

The brightest candidates are thus red. Self-enrichment models developed by Bailin & Harris (2009) predict a mass-metallicity relationship (MMR) for the most luminous globular clusters (with masses $> 10^6 M_\odot$). Due to self-enrichment blue massive globular clusters and UCDs are expected to migrate in color towards the red. The visible effect of this mass-metallicity relationship in the CMD is the truncation towards higher luminosities of the blue subpopulation of globular clusters and a red color for the brightest UCDs, as observed in Figure 6 and 8.

7. SPATIAL DISTRIBUTION

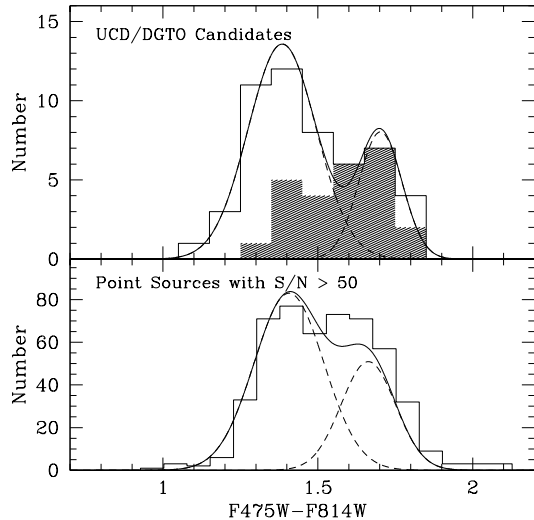


FIG. 8.— Top panel: Color distribution of 52 UCD/DGTO candidates. We also over-plot the best bimodal fit to the distribution. Each Gaussian describes the red and blue subpopulation. The mean color for the blue subpopulation is $\mu = 1.39$ with a dispersion of $\sigma = 0.11$ while the mean color for the red subpopulation is $\mu = 1.70$ and $\sigma = 0.07$. The shaded histogram corresponds to 25 UCD candidates, i.e. $M_V \lesssim -11$ mag. Bottom panel: color histogram for all 631 sources for which we attempt to derive structural parameters, i.e. objects with $S/N > 50$.

In Figure 9 we plot the spatial distribution of globular clusters, UCD/DGTO candidates and large galaxies in the ACS frame. At the Coma distance an ACS/WFC field of view covers an area of ~ 100 kpc². A clear over-density of globular clusters appears to be associated with NGC 4874 and to a lesser extent with NGC 4873. No over-density is visible around NGC 4871. In this image, NGC 4874 is off-center, towards the edge of the field of view. The adjacent ACS field was part of the original observing program but was not acquired due to the failure of the instrument. A definitive conclusion on the spatial distribution of UCD/DGTO candidates is difficult to reach without the missing adjacent field. With the available data we observe that UCD/DGTO candidates appear to congregate around NGC 4874 and more importantly their spatial distribution is not random. The non-uniformity of the spatial distribution of UCD/DGTO candidates and their colors argue against background sources masquerading as UCD/DGTOs.

The cumulative fraction of globular clusters and UCD/DGTO candidates as a function of radial distance to NGC 4874 is plotted in Figure 10. Both stellar systems follow the same distribution. In fact a formal two sample Kolmogorov-Smirnov test yields a maximum difference between the two, azimuthally averaged, cumulative distributions of $D = 0.14$ with a corresponding $P = 0.678$. This result is valid if we compare UCDs and GCs, the maximum difference in their cumulative fractions is $D = 0.15$ with $P = 0.724$, see Figure 10. In Figure 10 we also plot the surface density of compact stellar systems in the vicinity of NGC 4874. There is a deficit of UCD/DGTOs in the inner 15 kpc around NGC4874. This deficit of DGTOs and UCDs can be explained, at least in part, by tidal interactions with the host galaxy. At small galactocentric distances tidal interactions with the host galaxy destroy or truncate the size of large stel-

lar systems (Hodge 1960, 1962). For the Milky Way the relation between GC effective radius and galactocentric distance is $r_h \sim R_{gc}^{0.5}$ (van den Bergh et al. 1991). Similar relations have been found for several extragalactic GCS but using projected galactocentric distances (e.g. Jordán et al. 2005).

8. FINAL REMARKS

We do not observe any stark discontinuity between the characteristics of globular clusters, Dwarf Globular Transition Objects and Ultra-Compact Dwarfs in the core of the Coma Cluster. On the contrary, bright globular clusters, DGTO, and UCDs have similar luminosity, color, and effective radius. This is suggestive of a continuous distribution of stellar systems gradually increasing in size and luminosity (mass) from globular clusters to UCDs.

A spectroscopic survey is currently being carried out by Chiboucas et al. (2009); this project includes several of our UCD candidates as targets and will be the next obvious step to confirm the nature of our brighter detections.

We are grateful to J. Mack (STScI) for her continuous support of the ACS data analysis. K. Chiboucas (Gemini) shared with us results of her spectroscopic survey of Coma prior to publication, giving us greater insight to the data. We received advice from S. Larsen (Utrecht) on the optimum ISHAPE fitting radius. Many thanks to R. Cockcroft (McMaster) for contributing relevant references. This research has made use of the NASA Astrophysics Data System Bibliographic services (ADS), the NASA/IPAC Extragalactic Database (NED), and Google. STSDAS and PyRAF are products of the Space Telescope Science Institute, which is operated by AURA for NASA. We thank the anonymous referee for a constructive report and a prompt reply.

Facilities: HST (ACS)

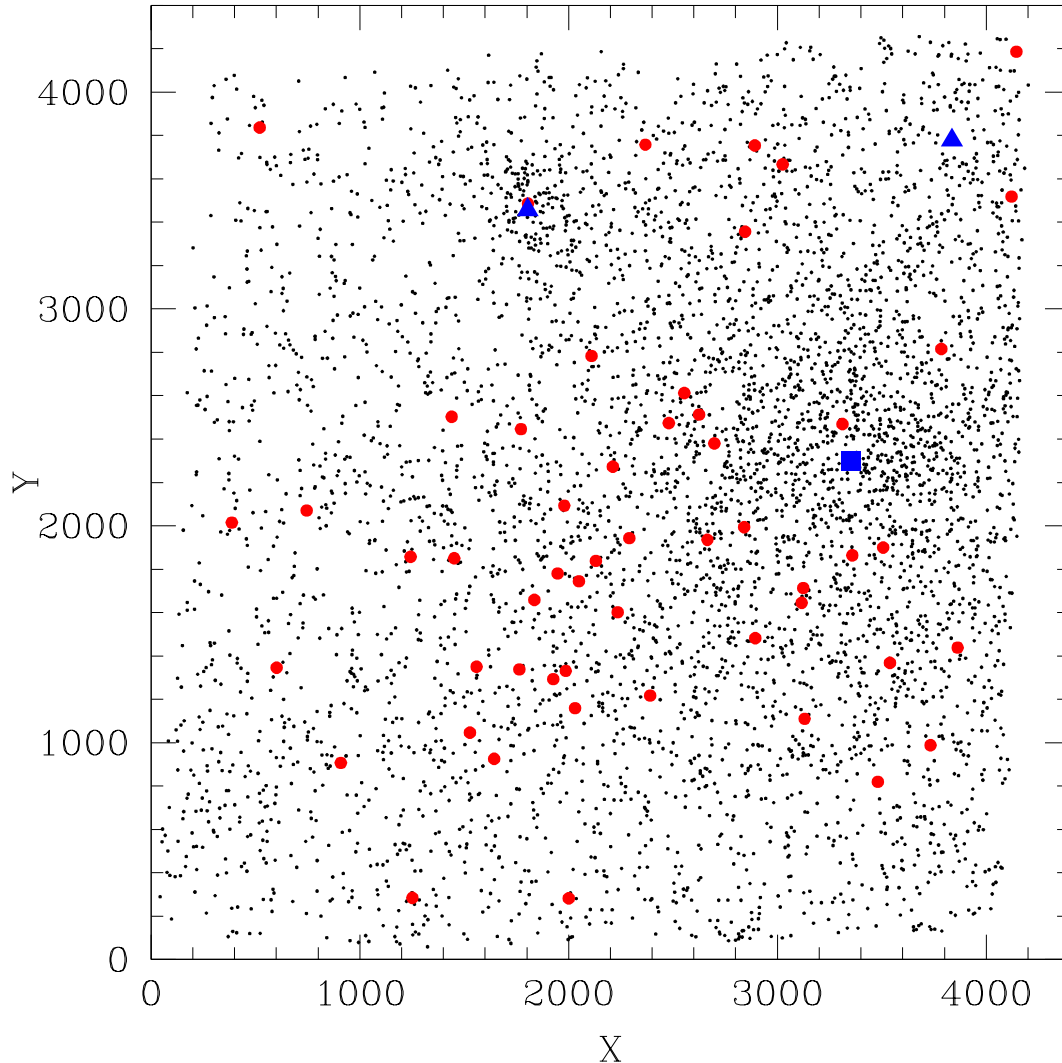


FIG. 9.— Spatial distribution of globular clusters (black dots) and UCD/DGTO candidates (red circles) around NGC 4874 (solid square). An overdensity of globular clusters is clearly visible surrounding NGC 4874. A second overdensity is associated with NGC 4873 (solid triangle, top middle). NGC 4871 (triangle, top right) appears to lack a corresponding globular cluster system. UCD/DGTO candidates are anisotropically distributed in the vicinity of NGC 4874. The units are pixels of the ACS/WFC camera.

REFERENCES

- Bailin, J. & Harris, W. E. 2009, *ApJ*, 695, 1082
 Blakeslee, J. P. & Barber DeGraaff, R. 2008, *AJ*, 136, 2295
 Blakeslee, J. P. & Tonry, J. L. 1995, *ApJ*, 442, 579
 Bertin, E., & Arnouts, S. 1996, *A&AS*, 117, 393
 Buzzoni, A. 2005, *MNRAS*, 361, 725
 Carter, D., et al. 2008, *ApJS*, 176, 424
 Chiboucas, K., et al. 2009, *BAAS*, 41, 234
 Chilingarian I. V. & Mamon, G. A. 2008, *MNRAS*, 385, L83
 Colless, M. 2001, *Coma Cluster in Encyclopedia of Astronomy and Astrophysics*, Nature Publishing Group, Basingstoke, UK
 Dabringhausen, J., Hilker, M., & Kroupa, P. 2008, *MNRAS*, 386, 864
 Drinkwater, M. J. et al. 2000, *PASA*, 17, 227
 Drinkwater, M. J. et al. 2003, *Nature*, 423, 519
 Dirsch, B. et al. 2003, *AJ*, 125, 1908
 Evstigneeva, E. A. et al. 2008, *AJ*, 136, 461
 Forbes, D. A. et al. 2008, *MNRAS*, 389, 1924
 Hammer, D. et al. arXiv:1005.3300
 Harris, W. E. 1996, *AJ*, 112, 1487
 Harris, W. E. 2009a, *ApJ*, 699, 254
 Harris, W. E. 2009a, *ApJ*, 699, 254
 Harris, W. E. 2009b, *ApJ*, 703, 939
 Harris, W. E., et al. 2009, *AJ*, 137, 3314
 Harris, W. E., et al. 2010, *MNRAS*, 401, 1965
 Hasegan, M., et al. 2005, *ApJ*, 627, 203
 Hau, G. K., et al. 2009, *MNRAS*, 394, L97
 Hilker, M., et al. 1999, *A&AS*, 134, 75
 Hilker, M. 2006, *UCDs- A mix bag of objects*, in *ESO Astrophysics Symposia: Globular Clusters Guides to Galaxies*, Springer, Berlin
 Hodge, P. W. 1960, *ApJ*, 131, 351
 Hodge, P. W. 1962, *PASP*, 74, 248
 Jordán, A. 2004, *ApJ*, 613, L117
 Jordán, A., et al. 2005, *ApJ*, 634, 1002
 King, I. R. 1962, *AJ*, 67, 471
 King, I. R. 1966, *AJ*, 71, 64
 Koekemoer, A. M., Fruchter, A. S., Hook, R. N., & Hack, W. 2002, in *The 2002 HST Calibration Workshop: Hubble after the Installation of the ACS and the NICMOS Cooling System*, ed. S. Arribas, A. Koekemoer, & B. Whitmore, Baltimore, STScI, 339
 Larsen, S. S. 1999, *A&AS*, 139, 393
 Larsen, S. S. & Brodie 2003, *ApJ*, 593, 263
 Larsen, S. S., et al. 2001, *AJ*, 121, 2974

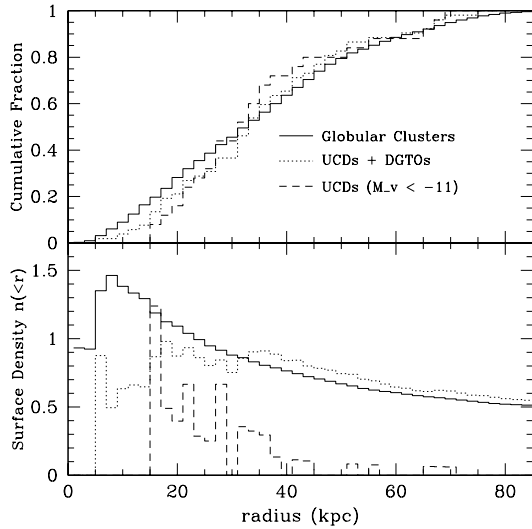


FIG. 10.— Top panel: Cumulative fraction of globular clusters, UCD/DGTOs, and UCD candidates as a function of radial distance to NGC 4874. K-S tests on these distributions show that the maximum difference in cumulative fraction between GCs and UCD/DGTOs is $D = 0.14$ with $P = 0.678$. Between GCs and UCDs these values are $D = 0.15$ and $P = 0.724$. Bottom panel: mean surface density of GCs, UCD/ DGTOs and UCDs. The surface density of UCD/DGTO and UCDs have been scaled by an arbitrary factor of 100 and 500 respectively.

- Larsen, S. S., et al. 2008, MNRAS, 383, 263
 Lee, M. G., et al. 2010, Science, 328, 334
 Mack, J., et al. 2003, ACS Data Handbook, Version 2.0, Baltimore, STScI
 Masters, K., et al. 2010, ApJ, 715, 1419
 Mieske, S., et al. 2004, AJ, 128, 1529
 Mieske, S., et al. 2006, AJ, 131, 2442
 Mieske, S., et al. 2007, A&A, 472, 111
 Mieske, S., et al. 2008, A&A, 487, 921
 Murray, N. 2009, ApJ, 691, 946
 Peng, E. W., et al. 2006, ApJ, 639, 95
 Peng, E. W., et al. 2008, ApJ, 703, 42
 Phillipps, S. et al. 2001, ApJ, 560, 201
 Price, J. et al. 2009, MNRAS, 397, 1816
 Romanowsky, A. J. et al. 2009, AJ, 137, 4956
 Sérsic, J. L. 1968, Atlas de Galaxias Australes (Córdoba: Observatorio Astronómico, Univ. Nac. Córdoba)
 Sirianni, M. et al. 2005, PASP, 117, 1049
 Sirianni, M., Gilliland, R., & Sembach, K. 2006 Technical Instrument Report ACS 2006-02, Baltimore, STScI
 Spitler, L. R. et al. 2006, AJ, 132, 1593
 van de Ven G. et al. 2006, A&A, 445, 513
 van den Bergh, S. et al. 1991, ApJ, 375, 594
 Wehner, E. M. H. & Harris, W. E. 2007, ApJ, 668, L35
 Wehner, E. M. H., et al. 2008, ApJ, 681, 1233
 William, B. F. et al. 2007, ApJ, 654, 835

TABLE 1
 POSITION, MAGNITUDE, COLOR, EFFECTIVE RADIUS, ELLIPTICITY, AND FITRAD OF UCD/DGTO CANDIDATES

X	Y	RA	Dec	m_{F814W}	Color	r_{hF475W}	r_{hF814W}	ϵ	$r_{h,circ}$	FITRAD
387	2015	12:59:39.22	27:59:54.7	19.76	1.74	41.9	47.7	0.28	40.5	15
2390	1217	12:59:40.60	27:58:08.4	21.14	1.70	34.0	36.8	0.22	28.7	15
1252	284	12:59:44.94	27:58:54.4	21.54	1.78	8.5	9.5	0.27	8.1	6
2894	1482	12:59:39.22	27:57:46.5	21.62	1.83	14.6	16.7	0.14	15.4	6
1979	2093	12:59:37.68	27:58:37.6	21.68	1.63	15.6	17.7	0.34	14.4	6
1836	1658	12:59:39.40	27:58:40.1	21.68	1.49	12.6	12.2	0.17	11.2	6
3130	1110	12:59:40.41	27:57:31.1	21.74	1.59	11.9	9.5	0.34	7.7	6
3481	819	12:59:41.21	27:57:10.9	21.77	1.60	11.2	11.9	0.20	10.6	6
2212	2273	12:59:36.83	27:58:28.1	21.81	1.72	10.5	10.5	0.24	9.2	6
1764	1338	12:59:40.64	27:58:40.3	21.90	1.63	8.8	12.2	0.15	11.3	6
1527	1046	12:59:41.91	27:58:48.9	22.06	1.51	6.1	11.2	0.03	11.1	6
2698	2380	12:59:36.06	27:58:05.4	22.07	1.70	16.0	20.1	0.18	18.2	6
2291	1943	12:59:37.99	27:58:20.8	22.10	1.42	24.1	26.5	0.32	21.9	6
2891	3754	12:59:30.83	27:58:10.2	22.26	1.45	6.5	9.9	0.27	8.4	6
2554	2612	12:59:35.31	27:58:14.9	22.33	1.66	54.1	66.0	0.04	64.7	15
2845	3357	12:59:32.33	27:58:08.4	22.40	1.84	9.9	11.2	0.11	10.6	6
2001	282	12:59:44.36	27:58:17.8	22.44	1.67	7.5	10.9	0.35	8.8	6
2031	1159	12:59:41.09	27:58:25.4	22.53	1.50	8.5	10.2	0.14	9.5	6
2625	2513	12:59:35.62	27:58:10.4	22.67	1.47	8.2	9.9	0.15	9.1	6
2235	1601	12:59:39.30	27:58:20.0	22.74	1.39	19.4	22.1	0.15	20.4	6
3785	2816	12:59:33.60	27:57:16.8	22.77	1.72	9.9	11.9	0.20	10.6	6
909	907	12:59:42.90	27:59:17.7	22.78	1.76	8.2	9.5	0.17	8.7	6
3863	1438	12:59:38.62	27:56:58.7	22.84	1.38	9.9	9.2	0.27	7.8	6
3539	1368	12:59:39.14	27:57:13.8	22.85	1.54	11.9	12.2	0.39	9.6	6
4121	3518	12:59:30.74	27:57:07.6	22.87	1.47	10.2	9.5	0.26	8.2	6
3124	1713	12:59:38.19	27:57:37.7	22.94	1.48	16.0	16.0	0.32	13.2	6
1440	2503	12:59:36.59	27:59:08.3	22.94	1.39	9.9	9.2	0.47	6.7	6
602	1346	12:59:41.52	27:59:37.2	23.00	1.44	26.6	31.7	0.14	29.4	15
746	2071	12:59:38.73	27:59:37.7	23.05	1.39	16.0	20.7	0.15	19.1	6
3507	1900	12:59:37.20	27:57:20.9	23.10	1.83	10.9	13.9	0.24	12.2	6
3359	1864	12:59:37.45	27:57:27.7	23.12	1.84	10.5	10.5	0.46	7.7	6
3311	2469	12:59:35.25	27:57:36.4	23.14	1.54	6.5	10.2	0.15	9.4	6
1559	1350	12:59:40.76	27:58:50.5	23.14	1.54	8.2	11.6	0.43	8.7	6
1644	925	12:59:42.26	27:58:41.9	23.26	1.36	6.1	9.9	0.43	7.4	6
2368	3758	12:59:31.23	27:58:35.9	23.27	1.47	12.2	13.9	0.40	10.8	6
3025	3667	12:59:31.05	27:58:02.8	23.34	1.43	9.2	10.5	0.20	9.4	6
520	3837	12:59:32.38	28:00:07.1	23.46	1.74	55.1	56.9	0.21	50.6	15
3733	988	12:59:40.39	27:57:00.4	23.56	1.39	11.9	12.9	0.38	10.2	6
2480	2474	12:59:35.88	27:58:17.1	23.58	1.49	10.2	12.2	0.11	11.5	6
2110	2783	12:59:35.03	27:58:38.4	23.59	1.19	17.7	11.9	0.36	9.5	6
3116	1645	12:59:38.44	27:57:37.4	23.61	1.34	23.8	30.3	0.16	27.7	6
4144	4187	12:59:28.25	27:57:13.4	23.82	1.54	11.9	13.3	0.24	11.6	6
1926	1293	12:59:40.68	27:58:31.9	23.92	1.28	21.4	18.0	0.15	16.6	6
2049	1744	12:59:38.92	27:58:30.6	23.92	1.76	10.9	9.2	0.44	6.9	6
2665	1936	12:59:37.72	27:58:02.4	23.95	1.38	50.0	58.2	0.28	49.4	15
1986	1331	12:59:40.49	27:58:29.4	23.96	1.45	24.8	39.2	0.38	24.9	6
2841	1994	12:59:37.37	27:57:54.4	24.00	1.29	16.7	19.4	0.14	18.0	6
1772	2446	12:59:36.54	27:58:51.4	24.01	1.32	11.2	14.3	0.26	12.3	6
1948	1780	12:59:38.86	27:58:35.9	24.03	1.29	9.2	13.6	0.49	9.7	6
1243	1857	12:59:39.13	27:59:11.2	24.07	1.54	18.7	9.2	0.45	6.8	6
1452	1850	12:59:38.99	27:59:00.9	24.16	1.33	12.2	11.9	0.12	11.2	6
2131	1838	12:59:38.51	27:58:27.6	24.22	1.34	14.6	12.9	0.28	11.0	6

NOTE. — Columns 1 & 2: x and y position in pixels of the ACS Camera; Columns 3 & 4: RA and Dec (J2000); Column 5: magnitude in the F814W band; Column 6: F475W-F814W color; Column 7: r_h in F475W in pc; Column 8: r_h in F814W in pc; Column 9: Ellipticity in F814W; Column 10 Circularized effective radius $r_{h,circ}$ (F814W) in pc; Column 11 FITRAD in pixels used for the given measurement